Batteries & Supercaps

Research Article
doi.org/10.1002/batt.202200441

Chemistry Europe
European Chemical Societies Publishing

www.batteries-supercaps.org

Full Cell Lithium-Ion Battery Manufacture by Electrophoretic Deposition

Gerard Bree[a] and Chee Tong John Low*[a]

Electrophoretic deposition (EPD) is a proven coating operation at an industrial scale. Initially designed for the automotive industry, it has expanded to other applications, notably ceramic coatings for surface protection, and has found promising application in the battery industry. Whilst fundamental half-cell studies of EPD electrodes are numerous, their practical performance at full-cell level is largely unknown. This study reports full-cell lithium-ion batteries in which anode and cathode are manufactured by EPD, using an exemplary $Li_4Ti_5O_{12}$/$LiFePO_4$ (LTO/LFP) chemistry. Investigations compatible with industry scalability were carried out including a) formulation of colloidal electrolytes for large area electrode manufacture, b) optimisation of EPD parameters providing high coating thickness and mass loading, c) comparison with slurry cast electrodes, d) scaling investigations to prototype large area pouch cells, and e) ease of manufacture with porous current collectors for high power applications. It was found that the practical performance of EPD electrodes outperformed slurry casting in various categories including lower resistances, more extractable capacity, higher power capability and stable cycling robustness.

Introduction

Electrophoretic deposition, commonly denoted by 'EPD' in the literature, is a coating process widely used in the automotive industry for corrosion protection. It is industrially popular as it offers the ability to deposit a uniform coating over an entire component, no matter how small or large, including those with bends, cavities or complex 3D structures which would be hard to coat with a conventional powder coat or wet painting process. It has also found important applications in other sectors such as ceramic coatings on leisure goods, domestic appliances and architectural components (e.g., aluminium, titanium, steel and other metal substrates). Industries are using EPD to produce underlayer coatings, in conjunction with other coating processes such as powder coating and electroplating, to build up multi-layered systems for a higher degree of tailored functionality. The EPD process continues to offer a wealth of possibilities to produce coatings with controlled properties (e.g., thin or thick, flat or rough, compact or porous, mono or graded layers) depending on the processing conditions. Although our comprehensive understanding of the underpinning mechanisms and fundamental electrochemical engineering aspects are far from complete, this has clearly not prevented EPD manufacturing technology on an industrial scale.

In recent years, the versatility of EPD process has expanded into the new sphere of manufacturing technology for electrochemical energy devices. It is receiving a high level of attention in academia, as well as by industry communities in many patents publications, as a modern tool to produce components of electrochemical energy devices. Many examples are recorded in the literature:

1) Energy storage electrodes in lithium-ion battery,[1–4] supercapacitor[5] and flow battery[6]
2) Solid-state electrolytes in solid oxide fuel cell[7]
3) Membrane electrode assembly in proton exchange fuel cell[8]
4) Photovoltaic electrodes in dye-sensitized solar cell[9]
5) Hydrogen production electrodes in water electrolyser[10]
6) Membrane separator in lithium-ion battery[11]
7) Ceramic-in-polymer electrolyte for lithium-ion battery[12]
8) Porous electrodes in structural lithium-ion battery[13]

For lithium-ion batteries, half-cell activities with small-area EPD electrodes have thus far been the focus for fundamental studies. The EPD electrode design have provided useful electronic, ionic and interfacial charge transports in lithium-ion battery applications. A detailed list of reported EPD battery electrodes is given in Table S1. Capacities close to the maximum theoretical values for the active materials were achieved, along with recorded improvements in other battery characteristics (e.g. lithium-ion diffusion coefficient, lower EIS resistances). A closer inspection of those reports, however, revealed that the extreme values of usable capacity and power capability are only achieved when mass loading of the electrode was very low e.g., $< 1\ mg\ cm^{-2}$. These high capacity values can be attributed to complete utilization of battery materials due to easy accessibility of electron and ion transport though the very thin layer to the current collector surface. While these fundamental studies of thin layers are useful for identifying the maximum achievable performance of battery materials, they are impractical for any real-world applications.

[a] Dr. G. Bree, Prof. C. Tong John Low
WMG, Warwick Electrochemical Engineering Group, Energy Innovation Centre
University of Warwick
Coventry, CV4 7AL, United Kingdom
E-mail: C.T.J.Low@warwick.ac.uk

Supporting information for this article is available on the WWW under https://doi.org/10.1002/batt.202200441

Another important challenge has been that these EPD electrodes were tested on coin cells scale only, specifically half-cell investigations using lithium counter electrode, which are too small and idealistic to be representative of practical devices (e.g., 21700 cylindrical cells, large format pouch cells and prismatic batteries). Crucially, many key engineering detrimental effects are masked at the small coin cells scale (e.g., flooded electrolyte to cover losses from SEI consumption, practically inexhaustible supply of cyclable Li). The research community has thus far focussed on the optimisation of electrode preparation process (formulation, deposition parameters, etc.) under these ideal conditions, with little attention to the commercialization requirements of thickness, cost and large-area full cell performance. It is therefore acknowledged that the practical performance of EPD energy storage electrodes at full cell and large device scale is largely unknown. This has limited our ability to prepare them for future scalability operation, and more manufacturing development in this area is required. The challenges associated with large-scale adoption of EPD in the lithium-ion battery industry would include the development of a low-cost, safe process which can produce uniform large-area electrodes with commercial-level mass loadings and thicknesses.

In our laboratory Warwick Electrochemical Engineering Group, United Kingdom, we have researched the practical aspects of EPD manufacturing technology for electrochemical technologies. Further reading can be found in our published articles for lithium-ion battery,[1] supercapacitor[5] and flow battery.[6] We now report the full-cell activity of lithium-ion battery in order to close the knowledge gap with existing half-cell studies, where both anode and cathode are manufactured by the EPD manufacturing technology. Given many industrial sectors continue to demand high power battery systems, we have chosen the high power and good safety characteristics of the LTO anode and LFP cathode system as an exemplary battery chemistry for these all-EPD electrodes full-cell investigations. LFP offers 170 $mAh\,g^{-1}$ theoretical capacity, with 175 $mAh\,g^{-1}$ for LTO. New variants of these materials are also possible, for example the higher power of niobium doped LTO[14] and higher capacity of manganese doped LFP.[15]

Key investigations from this study include:

1) Formulation of colloidal electrolytes that are suitable for large area manufacture,
2) Optimization of EPD parameters achieving commercially relevant coating thickness and mass loading,
3) Performance comparison with slurry casting electrodes,
4) Scaling investigations to A7 pouch cell for prototyping purpose,
5) Ease of manufacture with porous current collectors for high power applications.

The evidence provided in this article exemplifies EPD electrode manufacture with industry relevance. We hope this will help advance the manufacturing tools and processes of EPD electrodes from academic research a step closer to real-world industrial deployment. This approach is expected to be agnostic with respect to battery chemistry. More adventurous battery materials for future lithium-ion devices, for example high power 5 V LMNO and low cobalt NMC811 system, could reveal as yet undiscovered performance advantages of EPD and address the manufacturing constraints of slurry casting operation. The versatility of EPD continues to offer new scopes and technology advances for electrochemical energy devices, from solid-state battery to supercapacitor, fuel cell, water electrolyser and many more.

Results and Discussion

EPD process and the electrodes

In this work, we report an EPD process which utilises the inexpensive and non-toxic IPA solvent and $MgCl_2$ charging agent. The Mg^{2+} ion has been demonstrated to be an effective aid in the dispersion and deposition of both LTO[16] and LFP[17] through its adsorption onto the particle surface. Baths were prepared by dispersing active materials in the solvent, along with conductive carbon. Figure 1a shows a schematic of the EPD setup. Figure 1(b) shows the resultant coatings (60× 75 mm) were uniform, and the mass deposited could be controlled in a facile manner by modulation of the deposition time and deposition voltage. Figure 1(c) shows an image of an LFP electrode after a tape peel-off test, demonstrating the strong adhesion of the as-coated film (only a small amount of material is left on the adhesive tape). Figure 1(d), in which the electrode was bent 180° without any observed cracking or delamination, further demonstrating the strength of the EPD coating.

Optimization of EPD process

Table 1 shows the observed mass loadings and electrode discharge capacities for a series of depositions in which the bath recipe, specifically the content of CB, $MgCl_2$ and ethyl cellulose, concentration and the deposition time were varied. The addition of 10% CB brought about an almost 5-fold increase in electrode lithiation capacity, and was adopted for all deposition activities in our experiments. Increasing $MgCl_2$ content up to 5% led to an increase in deposited mass, attributed to an increased charge on the dispersed particles. Values greater than 5% reduced both deposited mass and electrode capacity, likely due to the formation of excess inactive (and insulating) deposits of $Mg(OH)_2$ and $Mg(C_3H_7O)_2$.[16] Therefore, a concentration of 5% MgCl2 was adopted balancing the formation of sufficient charge on the suspended particles while minimising inactive mass. An ethyl cellulose concentration of 5% was found to enhance colloidal stability and film adhesion while minimising inactive content and maintaining conductivity in the deposited LFP layer. Variation of the bath concentration and deposition time enabled facile modulation of observed mass loadings in the range 0.29 to7.58 $mg\,cm^{-2}$. Measurement of the zeta potential of a colloidal solution can provide useful information on its stability, as well as the response of suspended materials to the applied

Research Article
doi.org/10.1002/batt.202200441
Chemistry Europe
European Chemical Societies Publishing

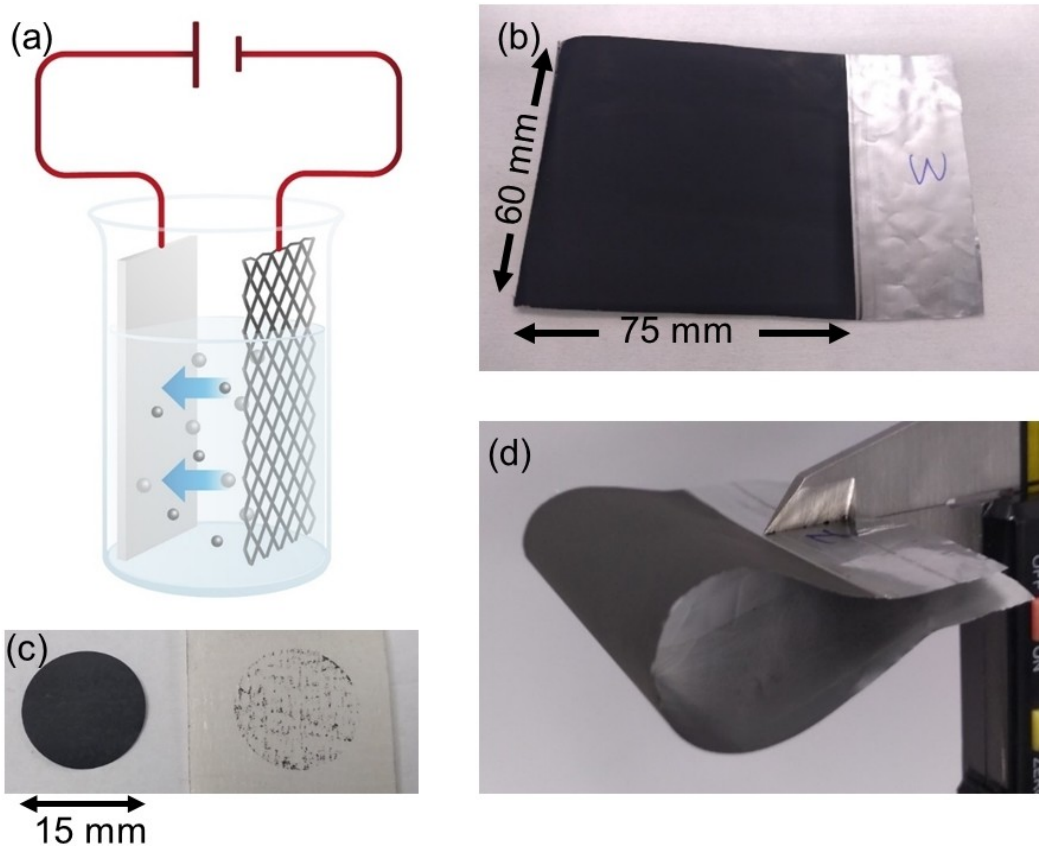

Figure 1. a) Schematic of the EPD setup, b) image of the 60×75 mm deposited LFP electrode, c) 15 mm diameter circular electrode disc and tape after the tape-off adhesion test. d) Electrode bent through 180° without cracking or delamination.

Table 1. Results of optimisation of EPD bath recipe and deposition parameters. Discharge capacity was measured in a coin cell using Li foil as both counter and reference electrode.

Component [wt%]	Mass loading [mg cm^{-2}]	Film thickness [μm]	Electrode discharge capacity [mAh g^{-1}]
Carbon black content (LTO)			
0%	0.80	16	25
10%	0.82	17	115
$MgCl_2$ content (LTO)			
2%	0.37	8	123
5%	0.82	17	125
10%	0.64	13	24
20%	0.41	9	6.7
Ethyl cellulose content (LFP)			
0%	0.28	7	124
5%	0.37	9	125
10%	0.42	9	77
Bath concentration (LTO, 5 min)			
1 g L^{-1}	0.53	11	118
2 g L^{-1}	1.75	19	99
5 g L^{-1}	4.49	64	107
Deposition time (LTO, 5 g L^{-1})			
2 min	1.51	20	134
5 min	2.20	42	113
10 min	6.13	90	107
15 min	7.58	115	76

Research Article
doi.org/10.1002/batt.202200441
Chemistry Europe
European Chemical Societies Publishing

electric field. Zeta potentials in excess of ±30 mV are required for adequate colloidal stability.[1,18] In our experiments, the measured zeta potentials of the active materials with charging agents were +39.6 mV and +7.39 mV for LTO and LFP, respectively. The beneficial effect of the addition of ethyl cellulose to the LFP bath is consistent with its lower zeta potential.

Microstructure of EPD electrodes

The microstructure of the EPD electrodes prior to cell assembly was assessed through SEM imaging. Figure 2 shows cross-sectional and top-down images of the LTO and LFP electrodes. The manufactured electrodes were sufficiently thick (30 μm) with commercially relevant and practical mass loadings (4 to 5 mg cm^{-2}). The images (coupled with EDS mapping) reveal active material particles well distributed throughout the thickness of the coating. It was observed that the conductive carbon particles (50 nm in diameter) have infiltrated the available spaces between the larger active materials, this strategic placement thereby provides the necessary electrical pathways through the entirety of the thick electrode coating. A closer view of the images, both cross-sectional and top surface microstructures (Figure 2c and d), showed an open pore network with tortuosity which extends from top to bottom of the thick electrode coatings, offering beneficial spacing for ions to move readily. Evidence in the literature of classical EPD research suggests that if the deposited coating is porous, which is the case here, the voltage drop across the layer will remain low. The availability of conductance pathways (both ionic and electrical) through the open porous structure offers the possibility to deposit an unlimited coating layer thickness from very thin nm to very thick mm. EDS elemental analysis (Table S3) confirmed the presence of active material, conductive carbon along with a small content of Mg. TGA (Figure S2) was employed to determine the ethyl cellulose content in the LFP electrode, with a value of 2.8% found.

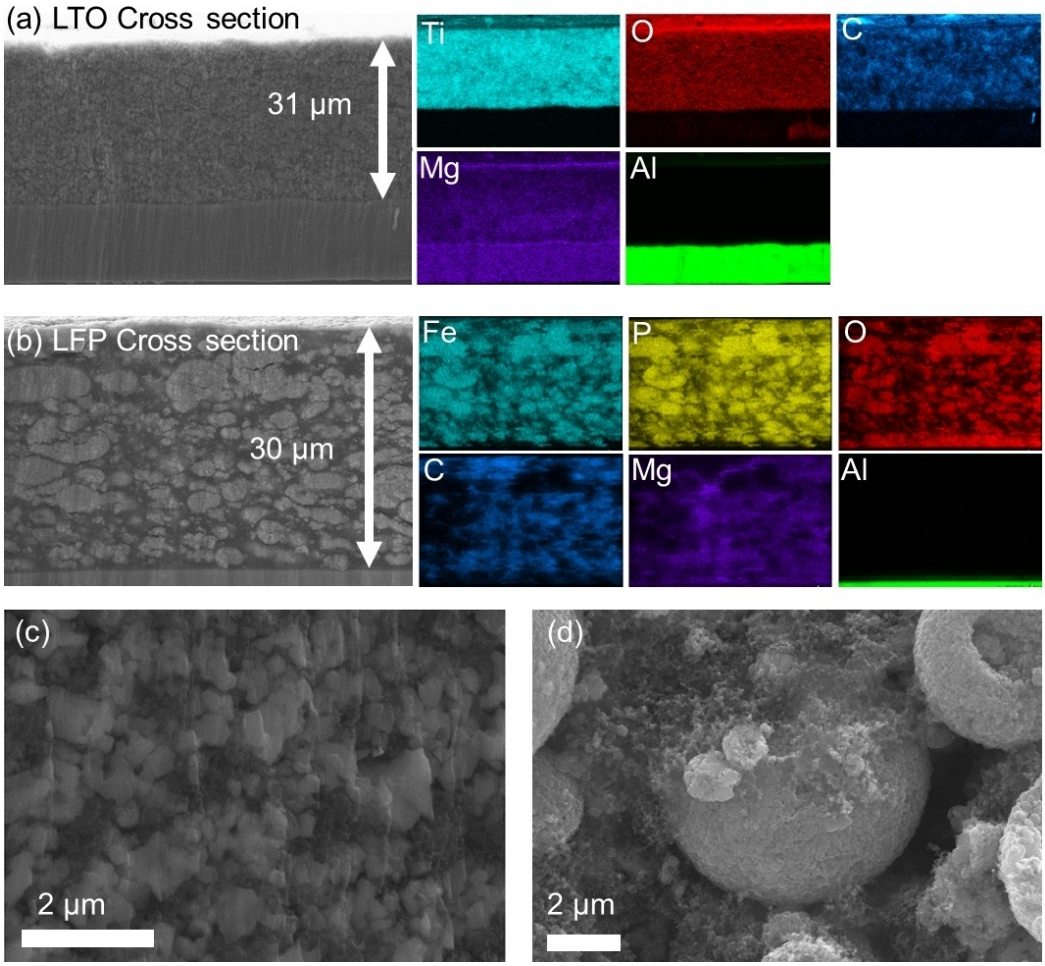

Figure 2. Cross sectional SEM images and EDS mapping of a) LTO and b) LFP electrodes deposited by EPD. Top-down SEM images of c) LTO and d) LFP electrodes showing microstructure of the active layer composite. The electrodes were fabricated using a bath concentration of 5 g L^{-1} with a deposition time of 5 min.

Research Article
doi.org/10.1002/batt.202200441
Chemistry Europe
European Chemical Societies Publishing

Electrochemical performance of EPD electrodes

Coin cell study

To assess the electrochemical performance of the EPD electrodes, as deposited LTO and LFP electrodes were assembled in 2032 coin cells, in both half cell (HC, using Li foil as both counter and reference electrode) and full cell (FC) configurations. Figure 3(a) shows the results of cyclic voltammetry (CV) analysis performed on HCs. The LTO electrode demonstrated clear cathodic and anodic peaks at 1.48 V and 1.68 V, respectively, attributed to the lithiation/delithiation of LTO, according to Reaction (1).[19] A similar CV scan of an LFP HC revealed lithiation and delithiation peaks at 3.33 V and 3.55 V vs. Li/Li^+, respectively, according to Equation (2).[20] For both materials, the distinct peaks and low peak separation was indicative of fast, reversible electrochemical processes and low cell impedance. The overall reaction of the LTO||LFP full cell is given in Equation (3) and cell voltage of 1.85 V.

$$\text{Anode } Li_4Ti_5O_{12} + 3Li^+ + 3e^- \leftrightarrow Li_7Ti_5O_{12} \quad E_{anode} = 1.55\ \text{V vs. } Li/Li^+ \tag{1}$$

$$\text{Cathode } LiFePO_4 \leftrightarrow FePO_4 + Li^+ + e^- \quad E_{cathode} = 3.4\ \text{V vs. } Li/Li^+ \tag{2}$$

$$\text{Full cell } Li_4Ti_5O_{12} + 3LiFePO_4 \leftrightarrow Li_7Ti_5O_{12} + 3FePO_4 \quad E_{cell} = 1.85\ \text{V} \tag{3}$$

Figure 3(b) shows the discharge capacity observed as LTO cell was galvanostatically cycled at a rate of C/5, compared with a similar cell assembled using an as-deposited slurry cast electrode. A high initial capacity (145 mAh g^{-1}) was observed for the EPD cell, along with little capacity loss after 100 cycles (144 mAh g^{-1}). This compares favourably with the slurry cell, which exhibited an initial capacity of 140 mAh g^{-1} (136 mAh g^{-1} after 100 cycles). The LFP HC (Figure 3c) similarly outperformed that manufactured by slurry casting. An initial capacity of 142 mAh g^{-1} was observed for the EPD cell, which compares favourably (>8 % advantage) with the slurry cell (initial capacity of 131 mAh g^{-1}). The EPD cell also exhibited superior capacity retention, maintaining 78% of initial capacity after 100 cycles. The capacity of the slurry cell, conversely, fell to < 10 mAh g^{-1} after 50 cycles.

The impedance spectra of the cells (Figure 3d) showed depressed semicircles, associated with charge transfer in the electrode, along with a straight line in the low frequency region, associated with Warburg diffusion in the electrolyte. The depression of the semicircles suggests the presence of multiple elements which overlap in frequency space, attributed to charge transfer within the electrode itself and across the electrode/current-collector interface.[21] Using the equivalent circuit shown in Figure S4, values for the series resistance "R1" (the sum of ohmic resistances) and the charge transfer resistances "R2" and "R3" were extracted from the spectra. Extracted values for R1, R2 and R3 were 3.5, 15 and 61 Ω (LTO) and 6.5, 3.8 and 134 Ω (LFP). Using Equation (3),[1] Li diffusion

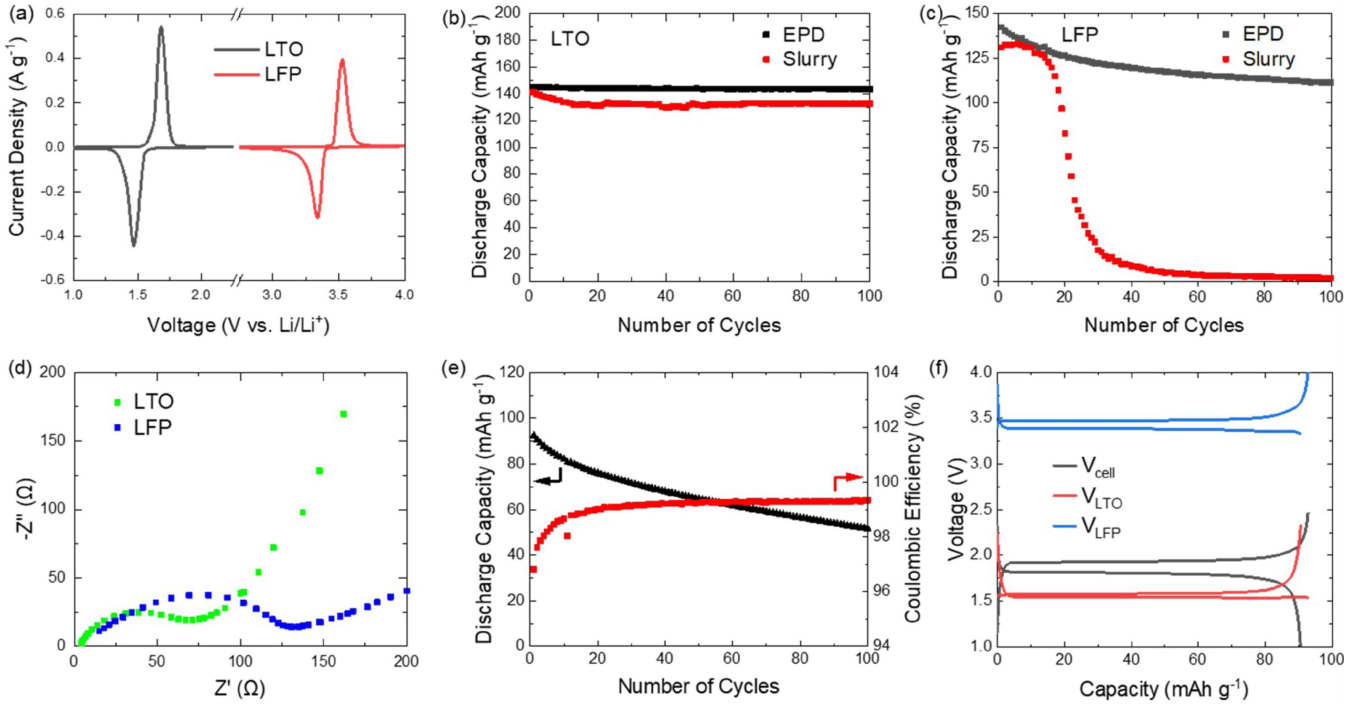

Figure 3. Electrochemical analysis of coin cells containing EPD electrodes (LFP and LTO). a) Cyclic voltammetry of half cells. b and c) Discharge capacity of half cells as a function of electrode active layer mass when cycled at C/5, compared with similar cells made using slurry casting. d) EIS analysis of LTO and LFP half cells (spectra were obtained in the discharged state). e) Discharge capacity and coulombic efficiency of an EPD full LFP||LTO cell. f) Voltage profiles of 3-electrode cell. A capacity ratio (N:P) of 1.15 was utilised (LTO excess), and capacities are defined relative to the mass of the limiting electrode. The electrode mass loadings were 0.2–0.3 mg cm^{-2} (HCs) and 1.0–1.1 mg cm^{-2} (FCs).

coefficients in the EPD electrodes were calculated to be 1.09×10^{-17} $cm^2 s^{-1}$ (LTO) and 3.24×10^{-15} $cm^2 s^{-1}$ (LFP).

$$D_{Li^+} = \frac{R^2T^2}{2A^2n^4F^4C^2\sigma_w^2} \quad (3)$$

where D_{Li+} is the Li^+ diffusion co-efficient, R is the gas constant (8.31 $J mol^{-1}$ K^{-1}), T is the temperature (293 K), A is the electrode area (1.77 cm^2), n is the number of electrons involved in the redox process (3 for LTO and 1 for LFP), F is Faraday's constant (96,485 C mol^{-1}), C is the Li^+ concentration in the electrode material (2.9×10^{-2} and 2.2×10^{-2} mol cm^{-3} for lithiated LTO and LFP, respectively), σ_w is the Warburg Impedance (Ω $s^{-0.5}$) co-efficient calculated from impedance spectra.

As discussed above, the HC format is useful in identifying the electrochemical processes and determination of maximum available capacity, however it is not necessarily reflective of practical electrode performance due to the presence of a large Li reservoir in the Li foil. Testing in a full cell configuration is necessary to validate this process for commercial use, and can reveal challenges which are not apparent from simple half-cell testing.[22] LTO and LFP EPD electrodes were assembled into a 3-electrode FC configuration (utilising Li foil as reference electrode), which enabled the monitoring of individual electrode potentials, as well as overall cell voltage. The FC exhibited an initial capacity of 92 mAh g^{-1} (Figure 3e), which was similar to that of an LFP HC made from the same deposition (97 mAh g^{-1}, see Figure S5). However, the capacity retention of the FC was inferior to the associated half cells, falling to 52 mAh g^{-1} after 100 cycles. This is attributed to the progressive consumption of cyclable Li in the FC,[22] with the coulombic efficiency lower than the corresponding HCs, particularly in the first 10 cycles. This variation in performance between HC and FC (and in particular the extra capacity loss in the FC) is consistent with previous lithium-ion battery studies and highlights the importance of testing in this configuration for the validation of EPD.[23] Figure 3(f) shows the individual potentials of the LFP and LTO electrodes in the FC in the first cycle, demonstrating the limiting nature of the LFP, i.e., the LFP fully delithiates (reaching 4 V vs. Li/Li^+), whereas the LTO is not completely lithiated (remaining at ~1.55 V vs. Li/Li^+). This situation was maintained at after 20 cycles (see Figure S5). The majority of full cell overpotential (131 mV at 50% SOC) was attributed to the LFP electrode (91 mV). EIS analysis (Figure S5) reveals a FC charge transfer resistance (530 Ω) slightly lower than the sum of the HC resistances (336 Ω and 278 Ω for LTO and LFP, respectively). This difference can be ascribed to the contribution from the Li foil in the HCs (which can be significant[22,24]).

Pouch cell study

To further demonstrate the viability of the EPD technique to commercial-type devices, a large area pouch cell was assembled utilising EPD as the sole deposition technique. To our knowledge, this is the first reported commercial-level lithium-ion battery device manufactured in this manner. Large LFP and LTO electrodes (60×75 mm deposition area) were produced by EPD, and then punched to pouch cell size (50×70 mm and 48×68 mm for anode and cathode, respectively (Figure 4a). The electrodes were calendered to achieve a density of 2 g cm^{-3}. Further information on the role of calendering is shown in the supporting information. These single-sided electrodes (with welded Al tags) were then assembled into a cell stack, and the completed pouch cell is shown in Figure 4(b). More details of the cell manufacturing process can be found in Figure S6. Electrochemical testing was carried out by mounting the pouch cells in custom testing jigs under controlled compression, simulating their use conditions in a commercial pouch cell pack.

Figure 4(c) shows the results of a rate capability test carried out on this pouch cell. The cell exhibited high capacity at low C-rates (115 mAh g^{-1} at C/5), surpassing the performance of the 3-electrode full coin cell. The cell also maintained good performance at higher C-rates (79 mAh g^{-1} at 2 C), indicative of the low resistance of the EPD electrodes. Repeated cycling at 2 C (Figure 4d) demonstrated the excellent stability of the EPD pouch cell, with capacity quite stable after the initial 10 cycles. EIS analysis (Figure S8) showed low Ohmic and charge transfer resistances of 0.10 and 9 Ω, respectively. These results clearly show that EPD can be readily adopted into existing lithium-ion battery cell assembly procedures while providing good cell performance.

Further performance enhancement using 3D foam current collectors

The benefit of 3D textured current collectors to lithium-ion battery performance has been demonstrated in several recent reports including Al,[25] Cu[4] and Ni[26] foams, embroidered Al,[27] and carbon fibers[13] (see review of existing literature in the Supporting Information). Through increased electrode surface area, and decreased Li^+ diffusion distances, significant enhancements in cell power density are possible,[28,29] as well as increases of mass loadings and areal capacities to values unachievable with standard planar foils.[25,27,30] These advantages span a wide range of lithium-ion battery materials, and also apply to next generation solid state devices.[31] However, the existing literature reports typically utilise vacuum-assisted slurry casting or high temperature processing steps, and thus industrial relevance is unclear. EPD, conversely, is inherently well suited to deposition onto 3D textured current collectors without the use of vacuum or high temperatures.[4] This combination may therefore yield the industrial relevance thus far lacking for EPD. Despite the potential of this combination, few studies in this area have been reported, and those utilise very low loadings and small cell areas in half-cell configurations.

In this work, the potential of a further enhancement to EPD performance through its combination with porous metal foam current collectors was investigated. Commercially available Al

Research Article
doi.org/10.1002/batt.202200441
Chemistry Europe
European Chemical Societies Publishing

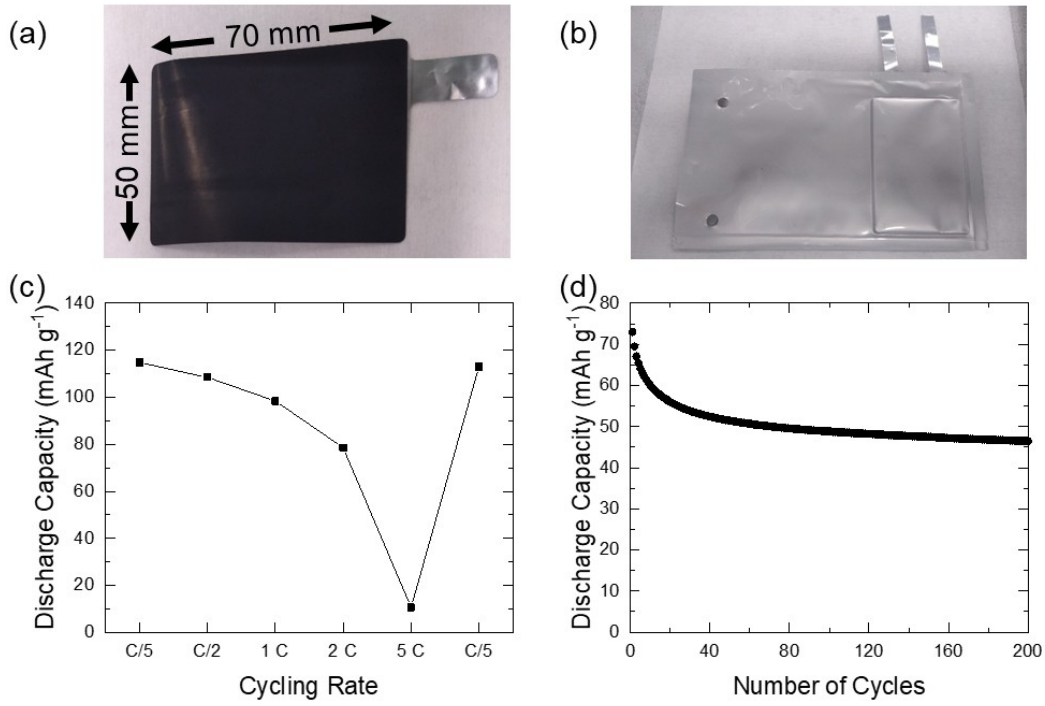

Figure 4. Commercial-style pouch cells manufactured by EPD. Photographs of a) LFP pouch cell electrode and b) completed pouch cell. c) Rate capability and d) repeated cycling at 2 C testing of the EPD pouch cell. An anode excess of approx. 10 % was utilised. Capacities are defined relative to the limiting electrode (LFP).

and Ni foam materials were chosen for cathode and anode, respectively. Al is traditional chosen as cathode current collector, while the utilisation of LTO as anode material enables the use of Ni foam instead of Cu foil. The pristine foams exhibited a porous structure (Figure 5c and e), advantageous for rapid Li^+ diffusion and low electrode resistance. The foams were pressed prior to deposition of active material (Figure S9), achieving the dual function of reducing the foam pore diameter into the range of typical thickness of battery active layers (50–250 μm), while also smoothing any rough edges, allowing the electrodes to easily be incorporated into standard coin and pouch cells. The thicknesses of the foam were reduced from 3.2 to 1.0 mm (Al) and 1.6 to 0.5 mm (Ni) (Table S6).

EPD of LFP onto Al foam and LTO onto Ni foam was carried out, with images of the resultant electrodes shown in Figure 5(a and b). Uniform coverage of the foam with active material was achieved at high mass loadings of 4.3 and 4.4 mg cm^{-2} for LFP and LTO, respectively. Top-down SEM imaging of the foam electrodes (Figure 5d and f) reveals uniform deposition and complete coverage of active material onto the foam. A cross sectional sample of the LTO/Ni foam electrode was prepared by broad beam ion milling to further examine its structure. Figure S10 shows an SEM image of the full thickness of the foam, confirming that active material is deposited throughout the thickness of the foam. Figure 5(g) shows cross-sectional SEM imaging and EDS mapping of individual strands of the Ni foam. EDS analysis confirms the complete coverage of the strands with active material (represented by the titanium and oxygen components). Conductive carbon is similarly found well-distributed in the pores of the foam. The presence of material completely filling the pores of the foam demonstrates the high throwing power of EPD, and the synergy between this deposition process and 3D current collectors. This is a significant step forward compared with previous slurry casting reports using foam architectures, (where a vacuum step is required to infiltrate the foam),[25] achieving both a reduction in processing complexity, cost and time.

Pouch cells utilising the foam electrodes were assembled in the next experiments. Al and Ni-coated Cu tags were welded directly onto the foam electrodes (Figure 6a and b), and the cell assembled into a stack. Electrochemical analysis was carried out as above, and performance was compared with a similar EPD pouch cell using Al foil as current collector. Figure 6(c) shows the discharge capacity (relative to cathode mass) of the 2 cells as a function of cycling rate. The superiority of the foam architecture at high charge-discharge rates is clearly visible, whereby the cell demonstrated an advantage over the foil cell at rates $\geq$ 2 C. The foam cell maintained 85 % of its low C-rate (1 C) capacity at 20 C (60 mAh g^{-1}), while the foil cell did not provide any capacity. Notably, the foam cell demonstrated cyclability at the very high rate of 50 C, fully discharging in $<$ 1 min. This confirms that the combined use of EPD foam architecture can bridge the gap between the traditional lithium-ion battery (high energy, low power) and capacitor (low energy, high power) modalities. The foam cell also exhibited superior capacity retention, as shown in Figure 6(d), in which the cells were repeatedly cycled at 5 C. Over 100 cycles, the foam cell degraded at just 0.05 %/cycle, compared with 0.28 %/

Research Article
doi.org/10.1002/batt.202200441
Chemistry Europe
European Chemical Societies Publishing

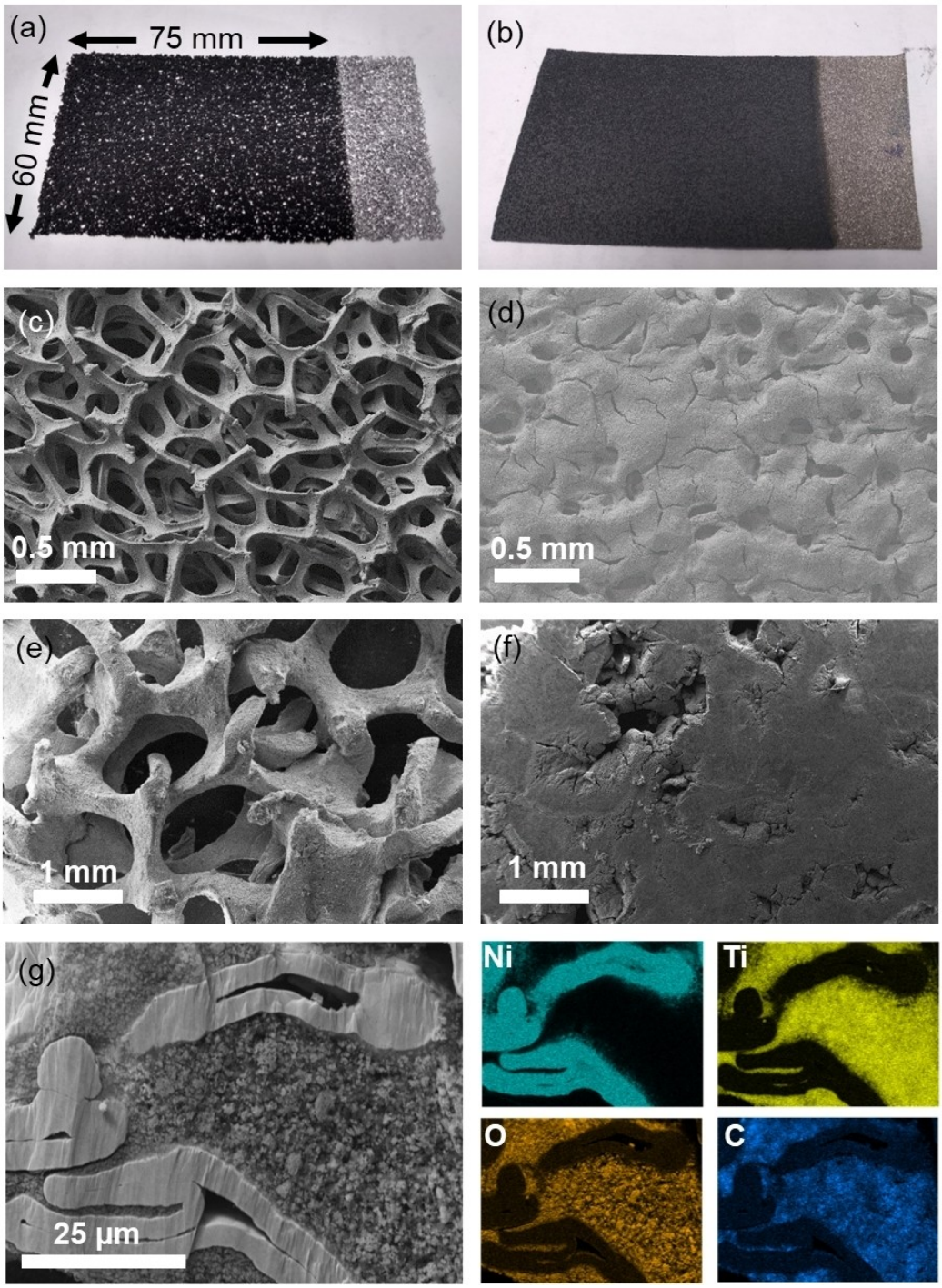

Figure 5. Photographs of a) LFP/Al foam and b) LTO\Ni foam electrodes manufactured by EPD. Top-down SEM images of c) pristine Ni foam, d) LTO/Ni foam electrode, e) pristine Al foam, and f) LFP/Al foam electrode. g) Cross sectional SEM image of LTO\Ni foam electrode with EDS mapping showing full penetration of active material into the porous foam. Active layer loading was in the range of 4–5 mg cm^{-2}.

cycle for the foil cell, confirming the robustness and good adhesion of the active materials onto the foam. The foam cell maintained an approx. 119% performance advantage over the foil cell throughout the duration of repeated cycling.

The superior performance at high charge-discharge rates was further examined by EIS analysis (Figure 6e). The cells exhibited similar ohmic resistance values (0.33 Ω and 0.28 Ω for foam and foil, respectively). However, a $>$25x reduction in the total charge transfer resistance of the foam cell (0.16 Ω) compared with foil (4.18 Ω) was observed. This dramatic difference can be attributed to the advantageous porosity of the foam architecture, with reduced Li^+ and e^- diffusion distances, and higher electrode surface area.

Research Article
doi.org/10.1002/batt.202200441
Chemistry Europe
European Chemical Societies Publishing

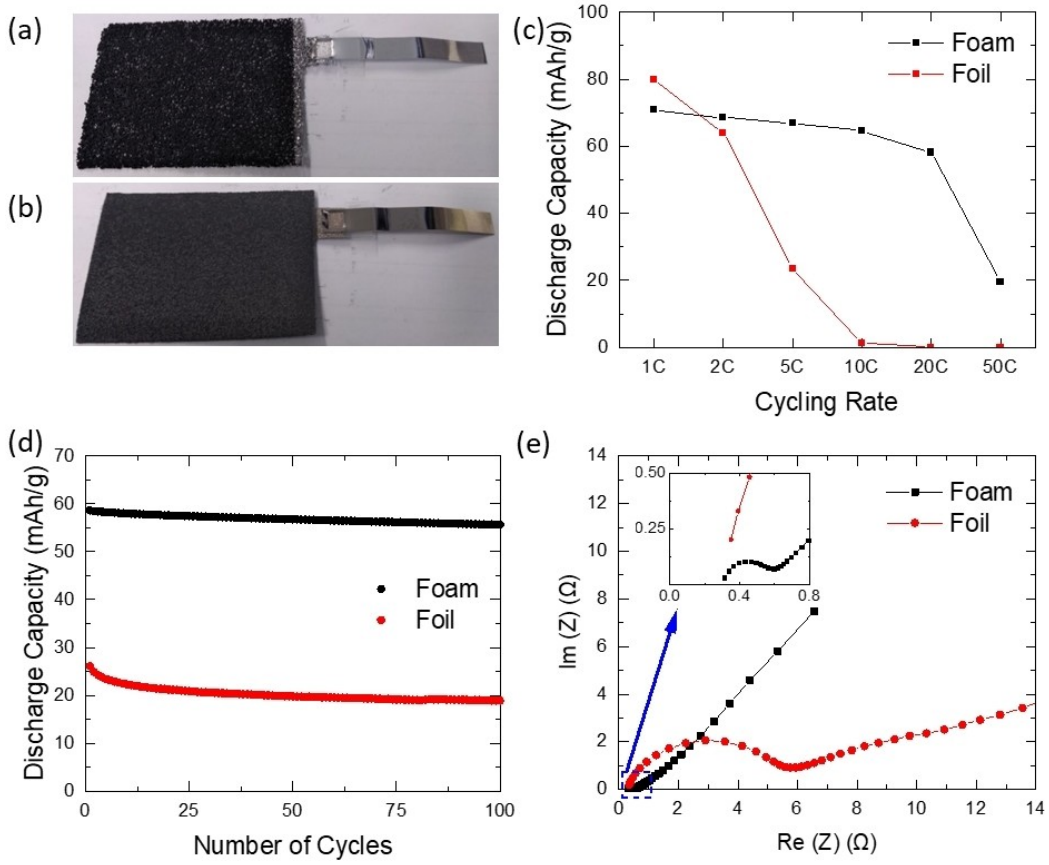

Figure 6. Images of a) LFP/Al foam pouch electrode, b) LTO/Ni foam electrode. c) Rate capability, d) repeated cycling at 5 C, and e) EIS of pouch cells manufactured by EPD, compared foam and foil current collectors.

Manufacturing considerations of EPD and slurry casting

All electrodes inside commercial lithium-ion batteries are currently produced by slurry casting. The process involves the mixing of battery active material powders with carbon black and binders to form a viscous slurry, which is then coated onto metallic foils and dried to produce high power and energy electrodes (20 to 100 μm thick with randomly distributed pores and material). Slurry casting has evolved to a highly productive, large scale industrial operation but is not without processing challenges. The following offers some insights into solving the slurry casting industry challenges through modern practices in EPD manufacturing and innovation.

Processing solvent. NMP is toxic to human reproduction and has been classified as a substance of very high concern (SVHC) and added to the European Union's REACH list of restricted substances.[32] This necessitates extensive safety procedures during its production and use. EPD can utilise alternative non-hazardous or lower hazard solvents such as IPA, water and acetone.

Electrode drying. The boiling point of NMP is 202 °C, while the value for IPA is 83 °C. The lower boiling point of EPD solvents means a lower drying temperature can be utilised. Thus, less energy is required during drying and solvent recovery processes. Shorter and less energy intensive drying steps would enable higher electrode throughput with shorter drying zones.

Electrode performance. The performance of slurry cast electrodes is limited by gradients in density formed during drying,[33] a challenge which is exacerbated at high film thicknesses and loadings.EPD makes use of a tunable electromotive driving force, and the density is controlled through the choice of deposition parameters. Furthermore, slurry casting is not well-suited to deposition onto 3D substrates, while EPD couples well with 3D porous and textured current collectors.[4,34]

To illustrate the potential manufacturing advantage of the proposed EPD process, the embedded energy and cost associated with solvent raw material, drying and recovery steps were calculated for the pouch cell electrodes produced in our investigations (Table 2). These three aspects represent a significant proportion (approx. 14.5 %) of total cell costs (see full breakdown for a typical cell in Figure S11). Data for NMP slurry casting were taken from a previous analysis,[35] which was adapted to the EPD process. For each process step, the % cost reduction associated with the switch from slurry casting to EPD was calculated (as shown in the last column of Table 2). The raw material cost of IPA is significantly lower (46 % at scale[36]) compared with NMP, while the much lower boiling point of IPA compared with NMP minimises the energy required to dry the electrode (93 % reduction) and recover the evaporated solvent

Table 2. Embedded energy and cost of solvent processing, comparing pouch cells manufactured by slurry casting and EPD. For ease of reading and relevance to commercial cells, figures are scaled to a 20-layer, double-sided pouch cell.

	Slurry casting with NMP		EPD with IPA		Cost reduction
	Energy [kWh]	Cost [$]	Energy [kWh]	Cost [$]	
Solvent cost	–	0.0053	–	0.0028	46%
drying	0.045	0.0045	0.003	0.0003	93%
recovery	0.156	0.0156	0.047	0.0047	70%
Total	**0.201**	**0.0254**	**0.051**	**0.0079**	**69%**

(70% reduction). Here we assume drying temperatures of 150 °C (NMP)[35] and 70 °C (IPA), and cooling to 35 °C during the recovery process. These factors amount to a cost saving of 69% associated with EPD during these process steps.

Conclusion

EPD is a well-established industrial production for surface coating and is currently finding increasing interests in the lithium-ion battery industry. Progressing EPD to the next stage of development to compete with traditional slurry casting requires researchers in this field to move beyond simple demonstrations of the process or proof-of-concept investigations. While the literature often shows high-performing EPD electrodes, these are frequently tested in idealised scenarios (low mass loading, small area electrodes, half-cell studies) and practical challenges associated with real-world industrial applications are ignored. Developing a greater understanding of the true benefits and limitations of this EPD process to real-world battery cells is the key next stage evidence enabling its adoption on an industrial scale.

In this research investigation, we have utilised the popular LTO||LFP chemistry as a model system to demonstrate the manufacture of large area, commercial scale EPD electrodes with high mass loading. The EPD bath recipe and deposition parameters were optimised for maximum performance, using cost-effective, non-toxic and commercially available components ($MgCl_2$, IPA, carbon black and cellulose binder). The EPD electrodes consisted of a dense film of active material particles dispersed within a conductive carbon matrix, contributing to high ionic and electrical charge transport. In conventional half-cell testing, the EPD electrodes achieved discharge capacities of 145 mAh g^{-1} (LTO) and 142 mAh g^{-1} (LFP), close to theoretical maximum, and outperformed similar slurry casted electrodes. Additionally, the EPD electrodes were more stable than their slurry counterparts under repeated cycling.

The lack of studies examining EPD in full cell configurations was addressed by assembling an all-EPD full coin cell, which demonstrated high initial capacity and good capacity retention over 100 cycles. Further optimisation of cell lithium content (through a pre-lithiation step) is likely to further enhance full cell EPD performance.

The challenge of translating promising coin cell results to large-area electrodes was addressed through the assembly of an all-EPD commercial pouch cell. The EPD cell exhibited a capacity of 115 mAh g^{-1} at C/5, maintaining 79 mAh g^{-1} at the higher cycling rate of 2 C. Pouch cell performance was further enhanced through the combination of EPD and porous metal foam current collectors, achieving a capacity of 60 mAh g^{-1} at the high rate of 20 C. The high throwing power of EPD enabled full penetration of the pores of the foam, creating an electrode with low resistance and high Li^+ diffusion. Finally, analysis of the energy usage during electrode manufacture revealed a cost reduction of 69% when utilising EPD in place of traditional slurry casting, benefitting from the lower cost, toxicity and boiling point of the EPD solvent.

The processes developed in this work showcase the excellent potential and versatility of EPD to replace slurry casting as a more cost-effective, higher performance manufacturing technique for all lithium-ion battery chemistries, as well as a wide variety of electrochemical energy storage device types. This work makes significant strides towards overcoming the challenge of moving EPD from lab to factory.

Experimental Details

Colloidal electrolytes recipes

Commercially available lithium-ion battery active materials LTO-1 (carbon coated) and LFP (A14, carbon coated) were obtained from Targray and ALEEES, respectively. Ethyl cellulose and $MgCl_2$ were obtained from Merck. SuperP carbon black was obtained from Alfa Aesar. IPA (99.9% purity) was obtained from Fisher Scientific. Particle size analysis was carried out with a Beckman-Coulter LS13 320 Laster Diffraction Analyzer using de-ionised water as a carrier.

Process parameters for EPD electrode manufacture

Lithium-ion battery electrodes were prepared by the EPD of electrode materials. In a typical process, the powders were dispersed in IPA at 1 g L^{-1}, alongside conductive carbon, ethyl cellulose and $MgCl_2$. The two formulations utilised were: 1) LTO (90%) and super P (10%), and 2) LFP (85%), super P (10%) and ethyl cellulose (5%). In both cases $MgCl_2$ was added as charging agent (5% of total solid mass). The colloidal electrolyte was then sonicated for 90 minutes, after which it was transferred to a beaker (100 mL for coin cell electrodes and 400 mL for larger pouch cell electrodes). The zeta potential of the colloidal electrolytes was measured using a Malvern Zetasizer Nano ZS (Malvern Instruments). The deposition substrate was formed by wrapping Al foil (MTI, 15 μm in thickness) around a suitably sized rigid substrate (glass or Al sheet). A platinum-coated titanium mesh (Magneto Special Anodes) was used as counter electrode and an inter-electrode distance of 10 mm was maintained throughout deposition. For porous substrates, free-standing Ni foam (MTI, 1.6 mm thick) or Al foam (Goodfellow, 3.2 mm thick was instead used, with

counter electrodes positioned either side of the foam to achieve double-sided deposition. After immersion in the bath, the Al foil was connected to the negative output of a DC power supply (Aim TTi PLH120 set to 90–120 V), and the platinised titanium to the positive. The bath was stirred at 100 rpm throughout deposition. After the desired deposition time (2–10 min) had elapsed, the voltage was switched off and the electrodes slowly removed from the bath, after which they were allowed to dry in ambient conditions. In some cases, a densification step was performed using a Gelon LIB calendaring machine, whereby films were compressed to approx. 70% of their initial thickness at 50 °C.

Coin and pouch cells assembly parameters

After drying and calendering, coin cell sized electrodes (15 mm anode and 14.8 mm cathode) were punched from the larger (50× 25 mm) films. Total deposited mass was determined by a microbalance (Sartorius SE2-F). The electrodes were stored at 60 °C in a vacuum oven overnight before cell assembly was carried out in an inert environment. Assembly of both full (LFP||LTO) and half (LFP||Li and LTO||Li) cells utilising 1 M LiPF6 in 1:1 ethylene carbonate: diethyl carbonate (Sigma Aldrich) as electrolyte and Celgard 2325 as separator was performed. Larger form pouch cells were assembled using a pilot cell assembly line. Briefly, larger electrodes (50×70 mm anode and 48×68 mm cathode, both with a 10× 20 mm uncoated tab area) were punched from the deposited films, after which external tags (0.2 mm thick ×8 mm wide, Al for cathode and Ni-coated Cu for anode) were ultrasonically welded onto the tab area. The electrodes were assembled into a "stack" along with 2325 separator and placed in a polymer-coated aluminium "pouch", which was then filled with electrolyte and sealed under vacuum (100 mbar).

Electrochemical testing protocols

Electrochemical testing was carried out using Biologic cell controllers (BCS & VMP, with a 5 A booster where required) in conjunction with the EC-Lab software. Coin cells were placed in Biologic CCH-1 four-point holders, whereas pouch cells were held in custom jigs, designed to replicate the stack pressure experienced in real world battery modules. Both cell types were held in an environmental chamber at 25 °C throughout testing. The analysis techniques included cyclic voltammetry, galvanostatic cycling and impedance spectroscopy.

Electrode analysis

Scanning electron microscope was performing using a Carl Zeiss Gemini. Energy-dispersive X-ray Spectroscopy (EDS) was carried out using an Oxford Aztec. Cross-sectional electrode samples were prepared by ion milling using Hitachi IM4000Plus Ion Milling. Thermogravimetric analysis (TGA) was carried out using a Perkin Elmer STA800.

Acknowledgements

This research has received financial support from the UK Government EPSRC Industrial Strategy Challenge Fund for the project "3D electrodes from 2D materials" (EP/R023034/1) and Engineering and Physical Sciences Research Council (EPSRC) First Grant: Energy Storage Electrode Manufacture (EP/P026818/1). Funding has enabled Prof. Low to initiate a research group and establish programmes from electrode to cell testing and recycling of lithium-ion batteries, as both Assistant Professor (2013) and Associate Professor (2019) in WMG, University of Warwick, United Kingdom. The world-class battery prototyping facility and resources of industrial relevance provided by the High Value Manufacturing Catapult at Warwick are acknowledged.

Conflict of Interest

The authors declare no conflict of interest.

Data Availability Statement

The data that support the findings of this study are available from the corresponding author upon reasonable request.

Keywords: Electrochemical engineering · electrophoretic deposition (EPD) · energy storage electrode manufacture · lithium-ion battery full cell

[1] C. C. Lalau, C. T. J. Low, *Batteries & Supercaps* **2019**, *2*, 551–559.
[2] G. Bree, H. Geaney, K. Stokes, K. M. Ryan, *J. Phys. Chem. C* **2018**, *122*, 20090–20098.
[3] B. K. Chakrabarti, M. Gençten, G. Bree, A. H. Dao, D. Mandler, C. T. J. Low, *Int. J. Energy Res.* **2022**, *46(10)*, 13205–13, doi:10.1002/er.8103.
[4] G. Bree, H. Geaney, K. M. Ryan, *ChemElectroChem* **2019**, *6*, 3049–3056.
[5] B. K. Chakrabarti, C. T. John Low, *RSC Adv.* **2021**, *11*, 20641–20650.
[6] B. K. Chakrabarti, J. Feng, E. Kalamaras, J. Rubio-Garcia, C. George, H. Luo, Y. Xia, V. Yufit, M. M. Titirici, C. T. J. Low, A. Kucernak, N. P. Brandon, *ACS Appl. Mater. Interfaces* **2020**, *12*, 53869–53878.
[7] S. M. Majhi, S. K. Behura, S. Bhattacharjee, B. P. Singh, T. K. Chongdar, N. M. Gokhale, L. Besra, *Int. J. Hydrogen Energy* **2011**, *36*, 14930–14935.
[8] H. Morikawa, N. Tsuihiji, T. Mitsui, K. Kanamura, *J. Electrochem. Soc.* **2004**, *151*, A1733.
[9] J. N. Nguu, B. O. Aduda, F. W. Nyongesa, R. J. Musembi, *J. Energy* **2014**, *8*, 757–764.
[10] A. Pozio, F. Bozza, N. Lisi, F. Mura, *Int. J. Energy Res.* **2022**, *46*, 952–963.
[11] J. Zhao, D. Chen, B. Boateng, G. Zeng, Y. Han, C. Zhen, J. B. Goodenough, W. He, *J. Power Sources* **2020**, *451*, 227773.
[12] T. He, G. Zeng, C. Feng, X. Jian, N. Chen, Y. Han, Q. Sun, D. Chen, S. X. Dou, W. He, *J. Power Sources* **2020**, *448*, 227469.
[13] J. S. Sanchez, J. Xu, Z. Xia, J. Sun, L. E. Asp, V. Palermo, *Compos. Sci. Technol.* **2021**, *208*, 108768.
[14] B. Tian, H. Xiang, L. Zhang, Z. Li, H. Wang, *Electrochim. Acta* **2010**, *55*, 5453–5458.
[15] L. Yang, W. Deng, W. Xu, Y. Tian, A. Wang, B. Wang, G. Zou, H. Hou, W. Deng, X. Ji, *J. Mater. Chem. A* **2021**, *9*, 14214–14232.
[16] N. A. Kyerematen, T. M. Dinh, D. Pech, *RSC Adv.* **2015**, *5*, 61502–61507.
[17] Y. Huang, H. Liu, Y. C. Lu, Y. Hou, Q. Li, *J. Power Sources* **2015**, *284*, 236–244.
[18] S. Kamble, S. Agrawal, S. Cherumukkil, V. Sharma, R. V. Jasra, P. Munshi, *ChemistrySelect* **2022**, *7*, DOI 10.1002/slct.202103084.
[19] C. P. Sandhya, B. John, C. Gouri, *Ionics* **2014**, *20*, 601–620.
[20] B. Özdogru, H. Dykes, S. Padwal, S. Harimkar, Ö. Çapraz, *Electrochim. Acta* **2020**, *353*, DOI 10.1016/j.electacta.2020.136594.
[21] F. Single, B. Horstmann, A. Latz, *J. Phys. Chem. C* **2019**, 23327–27343.
[22] H. Geaney, G. Bree, K. Stokes, K. McCarthy, T. Kennedy, K. M. K. M. Ryan, *J. Electrochem. Soc.* **2019**, *166*, A2784–A2790.
[23] B. Rowden, N. Garcia-Araez, *Energy Reports* **2021**, *7(2)*, 97–103, https://doi.org/10.1016/j.egyr.2021.02.048.
[24] K. Stokes, H. Geaney, G. Flynn, M. Sheehan, T. Kennedy, K. M. Ryan, *ACS Nano* **2017**, *11*, 10088–10096.
[25] M. Fritsch, G. Standke, C. Heubner, U. Langklotz, A. Michaelis, *J. Energy Storage* **2018**, *16*, 125–132.

[26] Q. Sa, Y. Wang, *J. Power Sources* **2012**, *208*, 46–51.
[27] N. Aguiló-Aguayo, P. P. Espiñeira, A. P. Manian, T. Bechtold, *RSC Adv.* **2016**, *6*, 69685–69690.
[28] N. Li, Z. Chen, W. Ren, F. Li, H. M. Cheng, *Proc. Natl. Acad. Sci. USA* **2012**, *109*, 17360–17365.
[29] C. U. Jeong, S. Y. Lee, J. Kim, K. Y. Cho, S. Yoon, *J. Power Sources* **2018**, *398*, 193–200.
[30] Z. Zhang, P. He, X. Li, Z. Yang, Y. Fu, Z. Lin, *J. Alloys Compd.* **2018**, *758*, 38–44.
[31] G. Zhang, B. Deng, Q. yao Liu, H. Yang, M. xiang Jing, S. Hussain, T. S. AlGarni, *J. Energy Storage* **2021**, *33*, 102167.
[32] "European Chemicals Agency - Substance Infocard, 1-methyl-2-pyrrolidone," can be found under https://www.echa.europa.eu/substance-information/-/substanceinfo/100.011.662, **n.d**.
[33] K. Kitada, H. Murayama, K. Fukuda, H. Arai, Y. Uchimoto, Z. Ogumi, E. Matsubara, *J. Power Sources* **2016**, *301*, 11–17.
[34] J. Hagberg, H. A. Maples, K. S. P. P. Alvim, J. Xu, W. Johannisson, A. Bismarck, D. Zenkert, G. Lindbergh, *Compos. Sci. Technol.* **2018**, *162*, 235–243.
[35] D. L. Wood, J. Li, C. Daniel, D. L. W. Iii, J. Li, C. Daniel, D. L. Wood, J. Li, C. Daniel, *J. Power Sources* **2015**, *275*, 234–242.
[36] W. Qi, R. Sathre, W. R. Morrow III, A. Shehabi, *Unit Price Scaling Trends for Chemical Products*, United States: N. p., **2015**, Web. doi:10.2172/1236367

Manuscript received: October 5, 2022
Revised manuscript received: November 17, 2022
Accepted manuscript online: November 21, 2022
Version of record online: December 21, 2022